Project no. **316488**

Project Acronym: KESTCELLS

Project title: Training for sustainable low cost PV technologies: development of kesterite based efficient solar cells. Industry-Academia Partnerships and Pathways

Start date of project: 01/09/2012

Duration: 48 months

Project coordinator: Dr. Edgardo Saucedo

Project coordinator organization name: IREC

Project website address: www.kestcells.eu

Deliverable D1.3
Electronic transport mechanism in CZTS and CZTSe kesterites: Role of defects

Delivery date: Month 38 (October 2015)

Dissemination Level:	PU
PU	Public
PP	Restricted to other programme participants (including the Commission Services)
RE	Restricted to a group specified by the consortium (including the Commission Services)
CO	Confidential, only for members of the consortium (including the Commission Services)

Document details:	
Workpackage	1: Fundamental properties of kesterites
Partners	UL, UAM
Authors	Eduard Garcia-Llamas (ESR1.2), Raquel Caballero, José Manuel Merino, Máximo León (UAM) Jan Sendler (ESR1.1), Susanne Siebentritt, Germain Rey (UL)
Document ID	D1.3
Release Date	Nov. 2015

Contents

1. Introduction and Summary

The transport properties of any semiconductor are closely related to the defects present in the material. They act as doping defects providing free charge carriers in the bands or as scattering centres that limit the mobility. At low temperatures the dominating transport mechanism can be entirely controlled by defects, namely when hopping of carriers between defect states becomes the main transport channel. Furthermore, defects do not only influence the transport properties, but they can also act as recombination centres and as such have a significant influence on the open circuit voltage of solar cells. The goal of this work is to correlate defects, transport properties and solar cell performance.

We use photoluminescence (PL) to study defects or – more general – the density of states in the band gap. In fact, it turned out that the radiative recombination of kesterites, independent of their preparation method and their composition is dominated by tail states, not by discrete defects. Tail states are also observed in other semiconductors, therefore we compared the effect of tail states in a semiconductor that shows good solar cells efficiencies, $CuInSe_2$, with the tail states of kesterite. The main observation is that tail states in kesterite dominate the radiative recombination. The extended bands do hardly contribute to the luminescence spectrum of kesterite. Thus the energy of the radiative recombination is lower than the band gap of the extended states and limits the open circuit voltage.

Nevertheless, an attempt was made to use classical semiconductor models to study the transport properties of kesterite single crystals. Two main observation were made: the activation energies of the conductivity are rather large and the low temperature transport is dominated by hopping. The high activation energies of the conductivity cannot be caused by the activation of the mobility across grain boundaries, since the measurements were performed at single crystals. Their high values thus indicate rather deep doping defects. For sulfides a decrease of the activiation energy with higher Ge content is observed, but not for selenides. The observation of hopping conduction indicates a rather high defect concentration. The transition temperature is lower for selenides, which can be attributed to a lower defect concentration as compared to sulfides.

2. Defects and tail states

ESR1.1's project is concentrating on the PL of kesterites. For this specific study we compared the PL, QE and absorption spectra measured by spectrophotometry of kesterites with those of chalcopyrite in an effort to characterise the influence of tail states. The work has already been published.[1] Figure A shows a comparison of the room temperature PL spectra of a $CuInSe_2$ and a $Cu_2ZnSnSe_4$ sample. We used $CuInSe_2$ for comparison to avoid problems of alloy disorder that will occur in $Cu(InGa)Se_2$ absorber. Our $CuInSe_2$ solar cells are 13.5% efficient.[2] For both samples we show the PL spectrum (light blue) and the quantum efficiency (QE) spectrum (red). The vertical lines depict the band gap of the extended states, as determined from a Tauc plot of the absorption spectrum, as well as the inflection point of the QE spectrum that is in literature often used to determine the band gap.

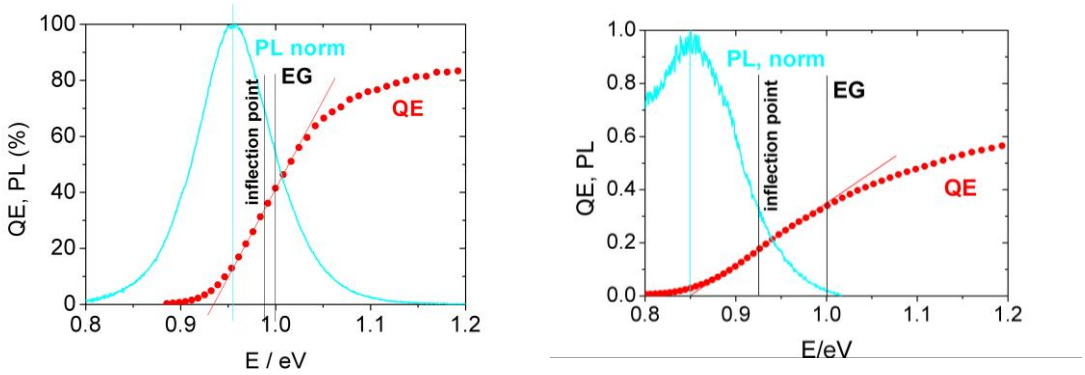

Figure A: Normalised PL spectra and quantum efficiency spectra of a $CuInSe_2$ absorber or solar cell (left) and a kesterite absorber or solar cell (right).

For the $CuInSe_2$ sample, the maximum of the PL spectrum is about 50 meV below the band gap of the extended states. The linear extrapolation of the QE spectrum extends to about the same energy below the gap of extended states. The PL emission spectrum extends well into the extended states above 1 eV. In the contrary, the PL spectrum of the kesterite sample extends essentially not above the gap of extended states. The maximum is 150 meV below the band gap. The linear extrapolation of the QE extends to the same energy. Both observations: the peak energy way below the band gap and no emission above the band gap, can be attributed to tail states with a high density of states, which extend into the gap and decay from the band edges. The tail states do contribute to the transport as is obvious from the QE spectra, most likely via the formation of a percolation path. Clearly, from the comparison between the $CuInSe_2$ and the $Cu_2ZnSnSe_4$ sample the tail states are much worse, i.e. extend to much lower energies in $Cu_2ZnSnSe_4$ than in $CuInSe_2$. Since the energy of the radiative recombination path in the bulk is the limiting value for the open-circuit voltage, it is obvious we lose already 100 mV of open circuit voltage by radiative recombination. Furthermore, the tail states are likely to increase Shockley-Read-Hall recombination and thus decrease the open-circuit voltage further. Thus it can be concluded that the tail states are a severe problem for the open-circuit voltage deficit in kesterite solar cells.

3. Direct investigation of transport properties

The work of ESR 1.2 involves the characterization of kesterite single crystals grown by Chemical Vapor Transport (CVT). The composition of the single crystals was determined by Energy-dispersive X-ray spectroscopy (EDX). X-Ray diffraction and Raman scattering were performed to assure the absence of secondary phases. Once the composition of the samples was known and confirmed the no presence of secondary phases, the transport properties of $Cu_2ZnSn_{1-x}Ge_xS_4$ and $Cu_2ZnSn_{1-y}Ge_ySe_4$ single crystals with x = 0.5, 0.7, 0.9, 1.0 and y = 0.3, 0.5, 0.7, 1.0 were investigated by conductivity vs temperature measurement.

3.1 Synthesis of single crystals

$Cu_2ZnSn_{1-x}Ge_xS_4$ (CZTGS) and $Cu_2ZnSn_{1-x}Ge_xSe_4$ (CZTGSe) single crystals were synthesized at the Belarusian State University of Informatics and Radioelectronics by chemical vapor transport (CVT) of the elements, using iodine as a transport agent [3]. Previously to the single crystal synthesis, the $Cu_2ZnSn_{1-x}Ge_xS_4$ compounds were grown by a modified Bridgman method, using elemental components with purities ≥ 99.999% inside a quartz ampoule under a vacuum pressure of 10^{-3} Pa. The CVT process was performed in another quartz ampoule filled with the grown compound and adding 5 mg cm^{-3} of iodine, located in a furnace with two independent heating zones. The temperature at the crystallization zone was kept at 970 K, around 80 K lower than the temperature at the reaction zone (1050 K), and both were maintained for 8 days [4] . Varying the amount of Ge and Sn, several $Cu_2ZnSn_{1-x}Ge_xS_4$ and $Cu_2ZnSn_{1-y}Ge_ySe_4$ single crystals with x = 0.5, 0.7, 0.9, 1.0 and y = 0.3, 0.5, 0.7, 1.0 were grown.

3.2 Compositional characterization of CZTGS and CZTGSe single crystals

The composition of the samples was measured by energy dispersive X-rays (EDX) (Oxford Instruments, model INCAx-sight) using a Hitachi S-3000N scanning electron microscope. The measurements were performed at 25 kV operating voltage and the Cu-, Zn-, Ge-, S, Se-K lines and Sn-L line were used. Tables 1 and 2 show the composition of the investigated samples. The relative error of the concentration values is 1% maximum.

Table 1. Composition of the $Cu_2ZnSn_{1-x}Ge_xS_4$ single crystals measured by EDX.

Sample	Cu (at%)	Zn (at%)	Sn (at%)	Ge (at%)	S (at%)	Cu/(Zn+IV)	Zn/IV	Ge/IV	S/M
Cu_2ZnGeS_4	26.95	11.38	--	11.08	50.59	1.20	1.03	1.00	1.02
$Cu_2ZnSn_{0.1}Ge_{0.9}S_4$	24.81	11.78	0.85	9.80	51.32	1.09	1.11	0.92	1.08
$Cu_2ZnSn_{0.3}Ge_{0.7}S_4$	27.18	11.90	3.39	8.48	49.05	1.14	1.00	0.71	0.96
$Cu_2ZnSn_{0.5}Ge_{0.5}S_4$	24.62	12.07	5.63	6.77	50.91	1.01	0.97	0.55	1.04

Note: M= Cu + Zn + Sn + Ge; IV = Sn + Ge

Table 2. Composition of the $Cu_2ZnSn_{1-x}Ge_xSe_4$ single crystals measured by EDX.

Sample	Cu (at%)	Zn (at%)	Sn (at%)	Ge (at%)	Se (at%)	Cu/(Zn+IV)	Zn/IV	Ge/IV	Se/M
$Cu_2ZnGeSe_4$	26.56	12.59	--	12.80	48.05	1.05	0.98	1.00	0.92
$Cu_2ZnSn_{0.3}Ge_{0.7}Se_4$	27.16	12.06	3.68	8.93	48.17	1.10	0.96	0.70	0.93
$Cu_2ZnSn_{0.5}Ge_{0.5}Se_4$	27.71	11.65	5.46	6.98	48.20	1.15	0.94	0.56	0.93
$Cu_2ZnSn_{0.7}Ge_{0.3}Se_4$	27.39	11.85	9.10	3.70	47.95	1.11	0.93	0.29	0.92

Note: M= Cu + Zn + Sn + Ge; IV = Sn + Ge

3.3 Secondary phases detection

X-ray Diffraction and Raman spectroscopy

Powder XRD diffractograms were performed in an X-Pert PRO θ-2θ device applying the geometry Bragg-Brentano using copper K-alpha1 (Cu Kα1) radiation. No secondary phases have been detected by XRD. However, it is not possible to completely discard the presence of secondary phases because of the high level of overlapping of the kesterite main Bragg peaks with Cu_2GeS_3, Cu_2GeSe_3, Cu_2SnS_3, Cu_2SnSe_3 ternary compounds and Zn(S,Se) binary compounds.

To assure the absence of secondary phases in the different CZTGS and CZTGSe compounds, systematic Raman scattering measurements were carried out. The Raman spectra were obtained with a Horiba Jobin Yvon LabRam HR800-UV matched with an Olympus metallographic microscope. Backscattering measurements were done with three different excitation wavelengths (532, 325, and 785 nm) focusing the laser spot onto the single crystal, and orientating the excitation light polarization along the crystal grown direction. The Raman spectra of all $CZT_{1-x}G_xS$ and $CZT_{1-x}G_xSe$ single crystals with different excitation wavelengths present excitation modes corresponding to single quaternary phases and did not present any secondary phase.

3.4 Transport properties

Conductivity versus temperature measurements

All single crystals were determined p-type by Seebeck measurements.

The conductivity, σ(T), was extracted from I/V measurements using the van der Pauw configuration in the temperature interval from 10 to 300 K. The contacts were made with silver paste.

The temperature dependence of the conductivity is shown in Figure 1. Two distinct behaviors are explicitly observed in two different temperature ranges. Therefore, it seems that different transport mechanisms can take place for these CZGTS and CZTGSe single crystals.

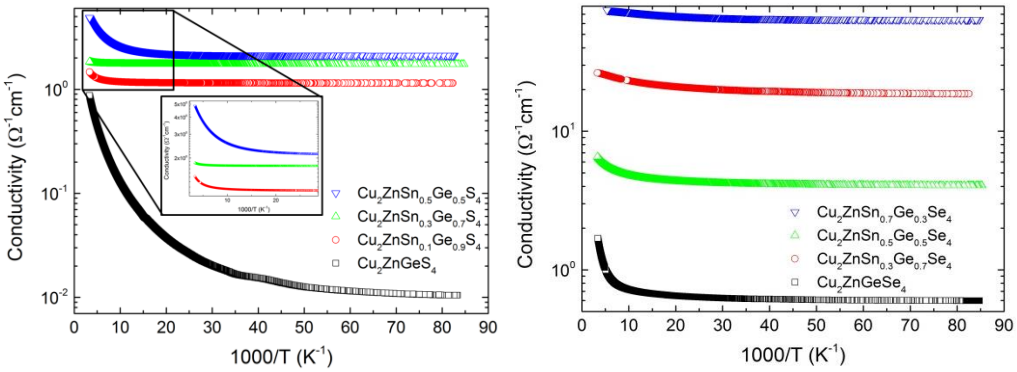

Figure 1. Temperature dependence of conductivity

The conductivity data σ can be quantitatively described by the equation:

$$\sigma(T) = \sigma_1 \exp\left(-\left[{}^{T_0}/_{T}\right]^{1/4}\right) + \sigma_2 exp\left(-{}^{E_2}/_{k_b T}\right) + \frac{\sigma_3}{T^{1/2}} exp\left(-{}^{E_3}/_{k_b T}\right) \quad (1)$$

where σ_1, σ_2, σ_3 are pre-factors, T_0 is the Mott characteristic temperature, k_b is the Boltzmann constant, E_2 is the nearest neighbor hopping activation energy and E_3 is the grain boundary barrier energy.

The first term of Eq. (1) denotes the Mott variable range hopping (M-VRH) on defects transport and the second term is the thermal activation (TA) conduction process. Transition from the TA to the M-VRH conduction regime takes place when it becomes energetically favorable for electrons to jump beyond the nearest-neighboring sites. Such situation is stimulated usually by lowering the temperature or increasing the microscopic disorder. The third term is related to the thermionic emission (TE) across grain boundaries. Here, the third term on the grain boundaries barrier is neglected because of the single crystal nature of the CZTGS and CZTGSe samples in this study. Then, Eq. (1) is rewritten to Eq. (2).

$$\sigma(T) = \sigma_1 \exp\left(-\left[{}^{T_0}/_{T}\right]^{1/4}\right) + \sigma_2 exp\left(-{}^{E_2}/_{k_b T}\right) \quad (2)$$

The experimental data were fitted with both possible models, M-VRH and TA. It appears that the TA model applies better in the high temperature range until 120 K and the VRH model applies better at lower interval temperatures from 120K. Figure 2 displays the variation of lnσ

vs 1000/T in the temperature range 120-300 K. As it follows from the second term of equation (2), equation (3), the plots of lnσ vs 1000/T in the interval of the thermal activation conduction process should be represented by linear functions. Therefore, the activation energies E_2 can be determined from the linear fits of these plots. Equation (3) is given by:

$$\sigma(T) = \sigma_2 \exp\left(-E_2 / k_b T\right) \quad (3)$$

After a visual inspection of the curves and regarding the correlation factors of the fittings, in most of the CZGTS compounds two linear fits with two different slopes were applied, the first one in the range of 310-215 K and the second between 160-120 K approximately. However, the experimental data have been fitted by only one linear fit in most of the CZTGSe single crystals with the exception of $Cu_2ZnGeSe_4$ that displays a different behaviour.

Table 3 shows the activation energies E_2 obtained for the different CZTGS samples. The E_2 values at the highest temperatures when two slopes can be considered show an increase when the Ge content is decreasing. On other hand, the E_2 values in the lower range of the high temperature region appear to decrease when the Ge content is increasing. These behaviours may be due to the presence of different Germanium defects. Up to our knowledge, no activation energies of Germanium related defects in the kesterite compound have been already determined, making more difficult to discern the kind of defects present in these samples

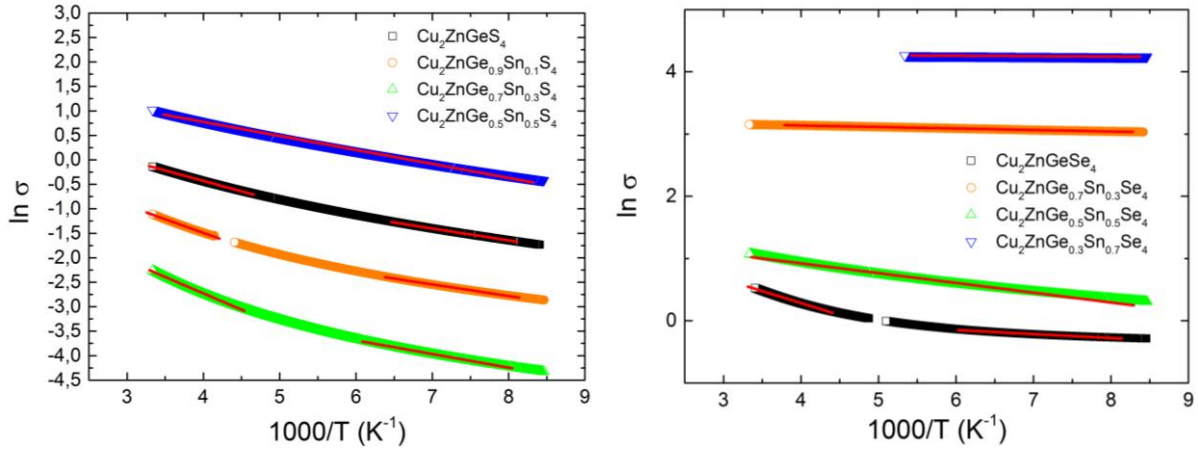

Figure 2. ln σ versus 1000/T. The red lines are the linear fits following the equation (3).

Table 3. Fitting parameters for the temperature dependent conductivity in CZTGS samples.

Sample	Thermal activation		
	$T_{initial}$	T_{final}	E_2 (meV)
Cu_2ZnGeS_4	215	311	36,76
	123	155	21,30
$Cu_2Zn\ Sn_{0.1}Ge_{0.9}S_4$	237	307	48,06
	123	157	20,41
$Cu_2Zn\ Sn_{0.3}Ge_{0.7}S_4$	220	310	57,52
	124	164	23,90
$Cu_2Zn\ Sn_{0.5}Ge_{0.5}S_4$	120	312	25,74

Table 4 shows the activation energies E_2 obtained for the CZTGSe samples. In this case, no correlation between the activation energy and Germanium content was found, apart from the lower obtained values compared to the case of the CZGTS samples

Table 4. Fitting parameters for the temperature dependent conductivity in CZTGSe samples.

Sample	Thermal activation		
	$T_{initial}$	T_{final}	E_2 (meV)
$Cu_2ZnGeSe_4$	227	302	33,18
	123	166	5,73
$Cu_2Zn\ Sn_{0.3}Ge_{0.7}Se_4$	124	301	2,11
$Cu_2Zn\ Sn_{0.5}Ge_{0.5}Se_4$	121	298	13,52
$Cu_2Zn\ Sn_{0.7}Ge_{0.3}Se_4$	121	288	2,09

Figure 3 shows the variation of lnσ with $T^{-1/4}$ in the temperature interval of 12-120 K. As mentioned above, the Mott variable range hopping fits better to the experimental results in this lower temperature range. According to [5] , the experimental data were linearly fitted using equation (4):

$$\sigma(T) = \sigma_1 \exp\left(-\left[T_0 / T\right]^{1/4}\right) \quad (4)$$

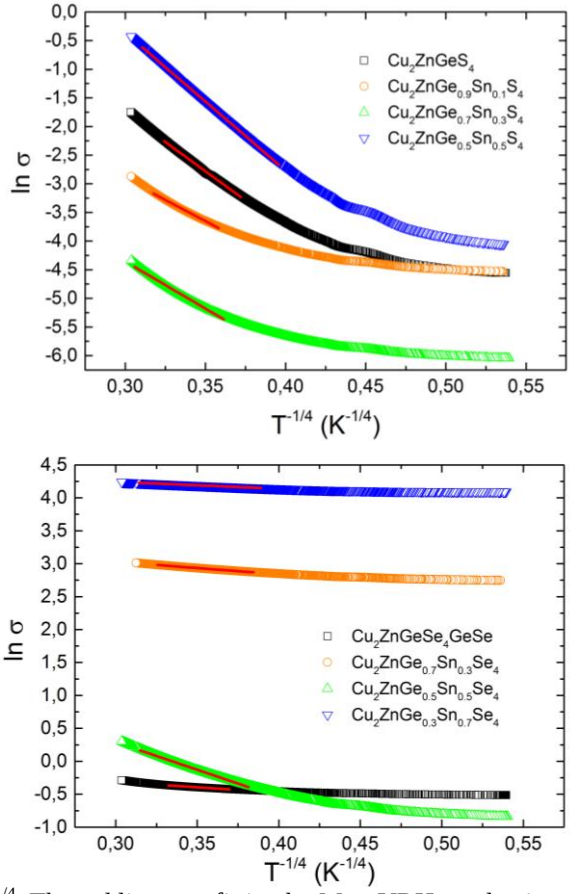

Figure 3. σ versus $T^{-1/4}$. The red lines are fitting by Mott VRH conduction mechanism by Eq. (4).

Table 5 shows the characteristic parameters of the Mott VHR conduction mechanism. Tv and Tm values are also included, which refer to the initial and final fitting temperature ranges respectively. T_0 is the characteristic M-VRH temperature, extracted from the fittings done following the Eq. 4, and the parameter W is the width of the acceptor band $W = (T_v^3 T_0)^{1/4}$ [6–8] .

In the Mott VRH interval, the band width of the band acceptor (W) has been found to vary between 27 to 34 meV for CZTGS, being similar to that reported [7]. For CZTGSe, there is more divergence in the band acceptor width, from 1.5 to 13.00 meV. The values of T_0, the Mott characteristic temperature, are inversely related to the density (DOS) of localized states near the Fermi level [9]. CZTGS samples show higher T_0 than those of CZTGSe, probably indicating that there is less density of localized states near the Fermi level for CZTGS [10].

Table 5. Fitting parameters of the temperature dependent conductivity for CZTGS and CZTGSe samples

Sample	M-VRH			
	T_0 (K)	T_v	T_m	W (meV)
Cu_2ZnGeS_4	$17{,}40 \times 10^4$	52,20	90,43	34,18
$Cu_2Zn\ Sn_{0.1}Ge_{0.9}S_4$	$4{,}75 \times 10^4$	60,73	98,33	27,68
$Cu_2Zn\ Sn_{0.3}Ge_{0.7}S_4$	$7{,}33 \times 10^4$	56,64	114,22	29,28
$Cu_2Zn\ Sn_{0.5}Ge_{0.5}S_4$	$33{,}51 \times 10^4$	40,71	107,28	33,42
$Cu_2ZnGeSe_4$	5,39	53,51	81,85	2,60
$Cu_2Zn\ Sn_{0.3}Ge_{0.7}Se_4$	12,38	45,80	88,84	2,85
$Cu_2Zn\ Sn_{0.5}Ge_{0.5}Se_4$	4892,88	47,30	101,53	13,00
$Cu_2Zn\ Sn_{0.7}Ge_{0.3}Se_4$	1,25	43,61	102,74	1,55

3.5 Conclusions

A first investigation of the transport properties of CZTGS and CZTGSe single crystals with different Ge-contents has been carried out. The samples were initially characterized by XRD and Raman spectroscopy to confirm the absence of secondary phases. Two different conduction mechanisms seem to take place for the single crystals, as observed in the variation of the conductivity with temperature. The thermal activated conduction process dominates at high temperature ranges, between 300 and 120 K, and the Mott variable range hopping fits better with the experimental results at lower temperatures, from 120 K to12 K. A decrease of the thermal activation energies with the Ge content seems to take place in CZGTS samples, while no clear dependence of activation energy is obtained with the Ge concentration in CZGTSe samples. The Mott temperature and width of the band acceptor are smaller for the CZTGSe single crystals than for the CZTGS samples.

4. References

[1] Susanne Siebentritt, Germain Rey, Ashley Finger, Jan Sendler, Thomas P. Weiss, David Regesch, and Tobias Bertram, Sol. Energy Mater. Sol. Cells doi:10.1016/j.solmat.2015.10.017 (2015).

[2] Tobias Bertram, Valérie Deprédurand, and Susanne Siebentritt, in 40th IEEE Photovoltaic Specialist Conference (IEEE, Denver, 2014), p. 3633.

[3] I. V. Bodnar, Growth and Properties of CuAlS2xSe2(1–x) Single Crystals, Inorg. Mater. 38 (2002) 647–651. doi:10.1023/A:1016271804632.

[4] R. Caballero, I. Victorov, R. Serna, J.M. Cano-Torres, C. Maffiotte, E. Garcia-Llamas, et al., Band-gap engineering of Cu2ZnSn1−xGexS4 single crystals and influence of the surface properties, Acta Mater. 79 (2014) 181–187. doi:10.1016/j.actamat.2014.06.040.

[5] A. Nagaoka, H. Miyake, T. Taniyama, K. Kakimoto, K. Yoshino, Correlation between intrinsic defects and electrical properties in the, Appl. Phys. Lett. 103 (2013) 112107.

[6] M. Guc, R. Caballero, K.G. Lisunov, N. López, E. Arushanov, J.M. Merino, et al., Disorder and variable-range hopping conductivity in Cu2ZnSnS4 thin films prepared by flash evaporation and post-thermal treatment, J. Alloys Compd. 596 (2014) 140–144. doi:10.1016/j.jallcom.2014.01.177.

[7] K.G. Lisunov, M. Guk, a. Nateprov, S. Levcenko, V. Tezlevan, E. Arushanov, Features of the acceptor band and properties of localized carriers from studies of the variable-range hopping conduction in single crystals of p-Cu2ZnSnS4, Sol. Energy Mater. Sol. Cells. 112 (2013) 127–133. doi:10.1016/j.solmat.2013.01.027.

[8] K.G. Lisunov, M. Guc, S. Levcenko, D. Dumcenco, Y.S. Huang, G. Gurieva, et al., Energy spectrum of near-edge holes and conduction mechanisms in Cu2ZnSiSe4 single crystals, J. Alloys Compd. 580 (2013) 481–486. doi:10.1016/j.jallcom.2013.06.156.

[9] N.F. Mott, E.A. Davis, Electronic processes in non-crystalline materials, 1971. doi:10.1016/0040-6090(72)90068-5.

[10] V. Kosyak, M.A. Karmarkar, M.A. Scarpulla, Temperature dependent conductivity of polycrystalline Cu 2 ZnSnS 4 thin films, Appl. Phys. Lett. 100 (2012) 1–6.